JACS Au
AN OPEN ACCESS JOURNAL OF THE AMERICAN CHEMICAL SOCIETY

pubs.acs.org/jacsau
Article

Flexible Pectin Nanopatterning Drives Cell Wall Organization in Plants

Oskar Siemianowski,* Sintu Rongpipi, Joshua T. Del Mundo, Guillaume Freychet, Mikhail Zhernenkov, Enrique D. Gomez, Esther W. Gomez, and Charles T. Anderson*

Cite This: JACS Au 2024, 4, 177−188
Read Online
ACCESS | Metrics & More | Article Recommendations | Supporting Information

ABSTRACT: Plant cell walls are abundant sources of materials and energy. Nevertheless, cell wall nanostructure, specifically how pectins interact with cellulose and hemicelluloses to construct a robust and flexible biomaterial, is poorly understood. X-ray scattering measurements are minimally invasive and can reveal ultrastructural, compositional, and physical properties of materials. Resonant X-ray scattering takes advantage of compositional differences by tuning the energy of the incident X-ray to absorption edges of specific elements in a material. Using Tender Resonant X-ray Scattering (TReXS) at the calcium K-edge to study hypocotyls of the model plant, *Arabidopsis thaliana*, we detected distinctive Ca features that we hypothesize correspond to previously unreported Ca-Homogalacturonan (Ca-HG) nanostructures. When Ca-HG structures were perturbed by chemical and enzymatic treatments, cellulose microfibrils were also rearranged. Moreover, Ca-HG nanostructure was altered in mutants with abnormal cellulose, pectin, or hemicellulose content. Our results indicate direct structural interlinks between components of the plant cell wall at the nanoscale and reveal mechanisms that underpin both the structural integrity of these components and the molecular architecture of the plant cell wall.

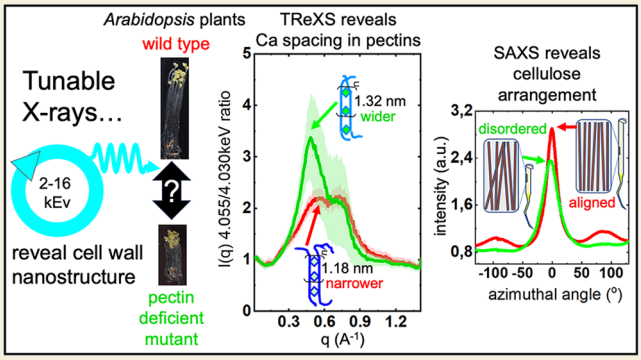

KEYWORDS: *Cell wall nanostructure, Tender resonant X-ray scattering, pectin, cellulose, xyloglucan*

INTRODUCTION

The mechanical properties of plant cell walls are determined by molecular interactions between rigid cellulose, branched hemicelluloses, and gel-like pectins; the latter two comprise the cell wall matrix. Each component has a specific abundance and architecture that contributes to cell wall structure and behaviors; for example, cellulose organization is thought to constrain cell growth directionality.[1,2] The organization and dimensions of cellulose microfibrils can be detected by various methods[3] and are critical for understanding many aspects of plant cell morphogenesis, including lobe formation in epidermal pavement cells,[4] tip growth in pollen tubes or root hairs,[5] or diffuse cell elongation as seen in etiolated hypocotyls.[6] Pectins can also have microfibrillar arrangements, and the organization of pectin nanodomains consisting of differentially methyl-esterified homogalacturonan (HG) has been hypothesized to influence wall stiffness and to even drive the expansion of specific wall regions during the anisotropic growth of epidermal cells.[7−9] Pectin molecular structure, which lies in the 1−5 nm range, is difficult to observe in intact cell walls by established methods, such as super-resolution optical microscopy, electron microscopy, NMR or X-ray diffraction,[10] but emerging approaches at the interface between materials science and biology could provide a new window into the structural complexity of plant cell walls, thereby opening the door for understanding and using an abundant but recalcitrant source of renewable bioenergy, high-value chemicals, and biomaterials.

X-ray scattering is a nondestructive analytical method that reveals the microstructure of materials.[11] Furthermore, using resonant X-ray Scattering leverages compositional differences in a given material by tuning incident X-ray energy within the soft (0.2 to 2 keV), tender (2 to 8 keV), or hard (>8 keV) X-ray regime at the absorption edges of specific elements.[3] Pectic HG differs from cellulose and hemicellulose in that it is negatively charged, and de-esterified galacturonic acid residues can be cross-linked by calcium ions (Ca^{2+}). X-ray scattering analysis at Ca absorption edges can enhance scattering contrast between Ca-cross-linked HG and other wall components, exposing Ca-specific features of the plant cell wall.[12] The application of Resonant Soft X-ray scattering (RSoXS) at the

Received: October 11, 2023
Revised: December 7, 2023
Accepted: December 13, 2023
Published: January 3, 2024

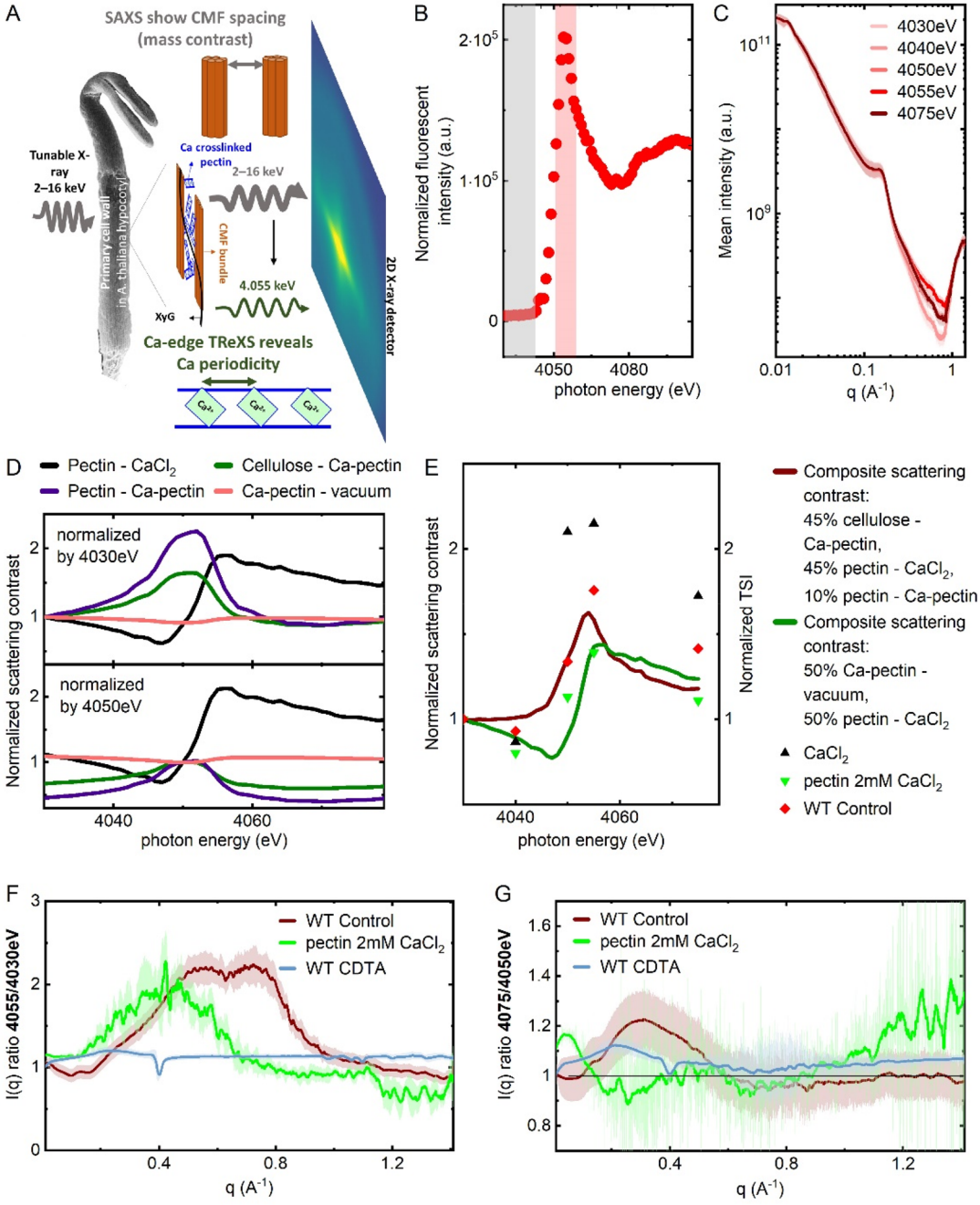

Figure 1. Tender resonant X-ray scattering reveals Ca dependent nanostructure in *A. thaliana* hypocotyls. (A) Resonant scattering at the Ca K-edge allows distinction of Ca and Ca-cross-linked pectin from other cell wall components. (B) NEXAFS profile of WT hypocotyls at the Ca K-edge with pre-edge energies highlighted in gray and the Ca K-edge in red. (C) $I(q)$ TReXS WAXS profiles at 4030, 4040, 4050, 4055, and 4075 eV. (D) Scattering contrast calculated for cell wall components, vacuum and Ca, normalized to 4030 eV (upper part) that shows Ca structures and 4050 eV (lower part) that deconvolute scattering contrast between Ca within carbon compounds (e.g., Ca-pectins) or Ca-pectin structures in cell wall components background. (E) Composite scattering contrast predictions and total scattering intensity (TSI between 0.2 and 1 A^{-1}) for WT control and Ca-pectin gel samples. (F, G) $I(q)$ 4055/4030 eV ratio and 4075/4050 eV for WT control, $CaCl_2$ and calcium cross-linked pectin dry gel, and hypocotyls treated with CDTA (pectin extraction). Shaded color above and under curves shows standard deviation of $n > 9$ measurements from 3 independent samples made of >15 dry hypocotyls.

Ca L-edge (~349 eV) in onion epidermal peels has revealed structures with a spacing of approximately 20 nm that were attributed to the average center-to-center distance between individual cellulose microfibrils or bundles of cellulose that are separated by the Ca-containing, pectin-rich matrix.[12] Tender Resonant X-ray Scattering (TReXS) at the Ca K-edge (~4055 eV) extends the accessible scattering vector (q) to detect features that include the crystalline planes of cellulose ($q \sim 1.5$ $Å^{-1}$).

Here, we use TReXS to detect Ca ordering that likely arises from Ca-HG nodes that are arranged in specific nanopatterns, which in turn underpin the unique physical properties and growth behaviors of plant cell walls. We also show that this ultrastructure defines interactions between pectins, cellulose, and hemicellulose and that alterations in pectin nanostructure

https://doi.org/10.1021/jacsau.3c00616
JACS Au 2024, 4, 177−188

help explain the origins of cell wall and growth disruptions in mutants lacking key wall components.

RESULTS

Nanopatterned Ca-HG Permeates Plant Cell Walls and Influences Primary Wall Structure

TReXS with wide angle detection at the Ca K-edge provides insight into nanostructures (0.45−50 nm) present in the plant cell wall and highlights those that contain Ca ions (Figure 1A). The presence of Ca leads to emission that can be observed by measuring the fluorescence yield by Near Edge X-ray Absorption Fine Structure (NEXAFS) spectroscopy. NEXAFS fluorescence spectra were recorded by scanning the energy from 4030 to 4150 eV with 1 eV resolution. NEXAFS spectra of dry hypocotyls of dark-grown *Arabidopsis thaliana* (*Arabidopsis*) seedlings showed a Ca K-edge starting at 4043 eV, with a maximum at 4055 eV and ending above 4075 eV (Figure 1B). When samples were treated with 2 mM $CaCl_2$, we observed enhanced Ca K-edge signals, indicating that native samples have unsaturated Ca sites (SI Figure 1).[13] Next, we performed transmission X-ray scattering across a range of energies, including two pre-edge (4030 and 4040 eV), two on-edge (4050 and 4055 eV), and one post edge (4075 eV). Scattering images at the center where the length scale is 10−100 nm (low q; in every case, we calculated d spacing from q using $d = 2\pi/q$) showed horizontal ellipsoid shapes as a result of mass contrast between dense cellulose microfibrils and the matrix. The elongated shape revealed cellulose anisotropy in the wall with a preferred microfibril alignment along the longitudinal growth axis (SI Figure 2). Both images showed an isotropic ring (SI Figure 2A,B), and radial integration profiles $I(q)$ (Figure 1C) revealed features at 3.49−5.24 nm ($q \sim 0.12-18$ Å^{-1}) that relate to the center-to-center spacing of cellulose microfibrils as described previously.[14−16] $I(q)$ profiles also indicated the presence of structure with $d \sim 1$ nm dimensions that might correspond to the size of cellobiose subunits in cellulose[17,18] or to spacing between pectin polymer chains. Additionally, at spacings of 0.57 nm ($q \sim 1$ Å^{-1}) and 0.43 nm ($q \sim 1.45$ Å^{-1}), we detected cellulose microfibril (CMF) (110)/(1−10) and (200) crystal planes (Figure 1C). Finally, we also observed a unique anisotropic signal at 6.28 nm ($q \sim 0.1$).[16] This feature is present only along the longitudinal axes of hypocotyls (SI Figure 3). All these features were clearly visible in hard X-ray (16.1 keV) scattering profiles, suggesting that contrast arises from mass heterogeneities in the samples (SI Figure 4).

Scattering intensity at the Ca edge (4055 eV) increased significantly compared to the pre-edge (4030 and 4040 eV) between 0.63 and 3.14 nm ($q \sim 0.2-1$ Å), indicating the presence of Ca-dependent features (Figure 1C). The width of the features suggests the presence of a broad structural size range (actual sizes of Ca domains or the distances between Ca domains), indicating the presence of Ca-dependent structures on this length scale. Additionally, the signal we analyze is gathered across hypocotyl tissues, including transverse and longitudinal cell walls. This increases the extent of observed features as we identify complex 3D structures. On the other hand, we have averaged information on the dominant cell wall structure. TReXS provides an opportunity to deconvolute the chemical identity of this feature. To do so, we compared total scattering intensities (TSIs) to theoretical predictions of scattering contrast. TSIs can be calculated using radially integrated $I(q)$ profiles at each energy (4030, 4040, 4050, 4055, and 4075 eV) near the Ca edge. Theoretical predictions of scattering contrast were calculated using a previously derived formula[19,20] with parameters derived from the Kramers−Kronig transformation (using kkcalc).[21] These predictions allow us to define broader conditions for TReXS analysis, showing what cell wall components can be distinguished at given photon energies.

We depict the predicted scattering contrast as a ratio of contrast at each energy to contrast at 4030 eV (Figure 1D). Contrast between Ca-containing structures and other materials increases close to the Ca K-edge and is minimal when no-Ca materials are compared (Figure 1D upper graph and SI Figure 5). The shape of the predicted scattering contrast also depends on component density.[21,22] Contrast curves between Ca-HG and other wall components have similar shapes (Figure 1D) and it is difficult to determine which materials are the source of the contrast. However, the contrast between pectin and $CaCl_2$ is higher than the contrast between cellulose and pectin cross-linked with Ca above 4060 eV (Figure 1D). Therefore, we normalized scattering contrast using the pre-edge energy of 4050 eV (Figure 1D lower graph) and based on that chose the 4075/4050 eV ratio to distinguish two distinct Ca environments: (i) ratio above 1, interpreted as Ca bound to a carbon compound, which in plant cell walls would most likely be pectin or Ca-binding cell wall proteins such as arabinogalactan proteins (AGPs). Because classical AGPs likely reside at the plasma membrane, they would potentially lose their organization (if any exists) in partially dried samples like ours. We interpret our data to mean that the detected Ca-dependent structures arise from pectin forming structures coordinated by Ca at substantial levels (the scattering contrast between pectin and Ca dominates). We refer to this as the Ca:polysaccharide signal, which can be interpreted as arising from the size or spacing between Ca atoms, e.g., in pectic Ca-eggbox units. The presence of Ca-eggbox in pectin within cell walls has been demonstrated in plants.[23,24] (ii) When the 4075/4050 eV ratio is below 1, this suggests that scattering arises from the distribution or size of polysaccharides that contain Ca, likely Ca-HG within cell wall components (scattering contrast between cellulose and Ca-containing pectin or between pectin and Ca-rich pectin dominates; see SI Figure 5B), and we refer to this regime as the Ca-HG:polysaccharide signal. The above conclusions are based on interpretation of theoretical scattering contrast and yield explanations for the observed data, although alternative interpretations are also possible.

Furthermore, assuming that plant cell walls are composite materials, we combined theoretical predictions of scattering contrast from cell wall components and matched them with TSIs from pectin or plants along the 0.2−1 A^{-1} q-range, where we observed a Ca dependent feature (Figure 1E). The TSI from TReXS analysis of Ca-cross-linked pectin gels matches a composite predicted scattering contrast with an even ratio of pectin:$CaCl_2$ and Ca-HG:vacuum. The vacuum interface is an artifact present in dried samples, potentially from the presence of nanopores or surface roughness. The experimental TSI for *Arabidopsis* hypocotyls compares well with a composite composed of nearly half of the predicted contrast arising from cellulose:Ca-HG (Figure 1E). Experimental data for neither cell walls nor Ca-HG gels match the scattering contrast predicted for pure $CaCl_2$ (Figure 1E). For comparison we also matched TSI at 0−0.1 A^{-1} (cellulose bundles); 0.1−0.2 A^{-1} (CMF q-range), and 1−1.4 A^{-1} (cellulose crystalline lattice)

https://doi.org/10.1021/jacsau.3c00616
JACS Au 2024, 4, 177−188

(SI Figure 5C) showing that scattering contrast is similar for Ca-pectin gel and *Arabidopsis* hypocotyls in the $q = 0.2-1$ A^{-1} range but not elsewhere. These results show that our predictions are corroborated by the experimental data.

The on-edge (4055 eV) to off-edge (4030 eV) ratio highlights the spacing of Ca-containing structures, as we have previously shown using a different energy range for polymer films.[25] We thus analyzed scattering data from plant cell walls and pectin gels using the on-Ca-edge to off-Ca-edge ratio (4055/4030 eV) and pre-Ca-edge to post-Ca-edge ratio (4075/4050 eV) to identify Ca-dependent features and distinguish whether they represent the Ca-HG structure itself or the spatial distribution of Ca-HG in the wall. First, in hypocotyl cell walls the 4055/4030 eV ratio revealed a Ca-dependent nanostructure with spacing between 1.10 and 1.21 nm ($q \sim 0.52-0.57$ $Å^{-1}$), hereafter referred to as the **dispersed** feature, and a smaller peak with spacing between 0.83 and 0.97 nm ($q \sim 0.65-0.76$ $Å^{-1}$), hereafter referred to as the **condensed** feature (Figure 1F). None of these features are visible when using hard X-rays in untreated or Ca-treated hypocotyls (SI Figure 4A,B). We assume that increased Ca signal at this q-range arises from overlapping Ca-dependent features and the feature appearance after dividing $I(q)$ profiles indicates a shift in the dominance of either dispersed or condensed features. The 4075/4050 eV ratio of scattering intensities from the hypocotyl cell wall is above 1, indicating that the size of Ca domains in pectin lies between 1 and 6 nm (Figure 1G). Only the dispersed Ca feature (4055/4030 eV) lies within this size range, suggesting this could be the predominant size of Ca egg-box structures.[24] In the size range of the condensed feature, the 4075/4050 eV ratio is smaller than 1 (Figure 1F,G). This could indicate contrast matching where approximately half of the signal comes from Ca domains in pectin, and the other half derives from Ca-HG structures in the cell wall.

Low methylesterified pectin cross-linked with 2 mM $CaCl_2$ showed Ca enhancement and a peak at 1.31−1.80 nm ($q \sim 0.35-0.48$ $Å^{-1}$) (Figure 1F). For comparison, the hydrated Ca-pectate unit cell viewed along the (100) direction would be spaced around 1.33 nm.[8] On average, the feature we observed in Ca-pectin gels was 0.1−0.4 nm larger than the dispersed feature detected in cell walls (Figure 1F). This smaller *in muro* Ca-HG structure might result from pectin interacting with relatively stiffer cellulose microfibrils that could slightly compress the pectin matrix. The Ca-pectin gel Ca:polysaccharide signal (4075/4050 eV > 1) is present for spacings higher than 4.3 nm, indicating a much larger dominant Ca structure than that in hypocotyl cell walls (Figure 1G). Such an increase in the size of Ca structures in isolated Ca-pectin gel could come from an increased freedom of egg-box structures to aggregate compared to *in muro* pectins. The signal from pure $CaCl_2$ increased at Ca K-edge energies, but no structures that resembled the ones detected in Ca-pectin gel or plants were present (SI Figure 6A, red curve). Consistent with its inability to cross-link via Ca, we also did not observe Ca-specific structures in highly methyl-esterified pectin (SI Figure 6A). We conclude that these Ca-dependent features are most likely related to the size of Ca-bound pectin substructures (condensed feature) and Ca-rich domains, possibly eggboxes, within pectin (dispersed feature), and therefore help to reveal pectin nanostructure in primary cell walls.

To test this hypothesis, we performed TReXS of *Arabidopsis* hypocotyls treated to reduce or increase the abundance of specific wall components. Unexpectedly, treatment of cell walls with chloroform, a nonpolar solvent that affects hydrophilic/hydrophobic interactions, caused not only removal of the cellulose microfibril feature (SI Figure 7A) but also caused the dispersed peak to adopt a 1.37−1.61 nm spacing, matching the feature detected in Ca-cross-linked pectin gels (SI Figure 6B,C). Furthermore, the peak in the $I(q)$ 4075/4050 eV ratio (above 1) also shifted to 1.37−1.61 nm spacing, the opposite direction from the feature in the 4055/4030 eV curve, suggesting a relaxation of the Ca-HG structure (SI Figure 6B,C). These results confirm not only that pectin interacts with cellulose microfibrils *in muro*[26] but also that this interaction influences the organization of both components. Moreover, because chloroform removes the cuticle, the presence of both dispersed and condensed features (although shifted) after the treatment indicates that they do not lie in the cuticle layer.

Pectin extraction with CDTA or total wall degradation with Driselase removed the Ca-specific 4055/4030 eV and cellulose peaks (Figure 1F; SI Figures 6B and 7), and also significantly reduced the Ca:polysaccharide signal (Figure 1G, SI Figure 6C). This suggests an interdependency of Ca-HG structure and the structural integrity of the cell wall. On the other hand, pectin demethyl-esterification via saponification by NaOH, which should increase the number of potential Ca binding sites, led to a significant intensity increase in a 4055/4030 eV Ca-specific signal with a spacing of 0.79−1.08 nm (SI Figure 6B), which roughly corresponds to the condensed feature in untreated hypocotyls (Figure 1F). Saponification shifted the Ca:polysaccharide signal feature peak from 2 to 6 nm (SI Figure 6C), with its position similar to the peak from Ca-pectin gels (Figure 1G). Likewise, the Ca-HG:polysaccharide signal (4075/4050 < 1) is much more pronounced in saponified cell walls (SI Figure 6C), consistent with the condensed Ca-HG 4055/4030 eV feature being related to the size of Ca-HG interspersed between cellulose microfibrils, and also suggesting a direct contact of low and highly methylesterified pectin with cellulose. Finally, saponification caused the disappearance of the cellulose peak, indicating that normal Ca-HG structure supports microfibril arrangement in the wall (SI Figure 7).

To further confirm that the observed features are Ca-specific, we exploited the ability of low methyl-esterified pectin to be cross-linked by cations other than Ca. WT hypocotyls were treated with Zn and La and analyzed at Ca, Zn, and La K-edges using TReXS (SI Figure 8). Adding Zn^{2+} or La^{3+} caused the Ca-dependent feature to shift to larger (Zn) or smaller (La) d-spacing, suggesting that these metals cross-link pectin, shaping it into more or less dense gel networks, respectively (SI Figure 8A). Moreover, the $I(q)$ profile ratio on vs off the Zn K-edge in Zn-treated samples indicates a prominent structure at larger spacing (~1.28 nm) (SI Figure 8A), but Ca treatment enhanced both dispersed (~1.21 nm) and condensed (~0.94 nm) features at the Ca K-edge (SI Figure 8B). TREXS on the Zn K-edge of Zn-treated samples indicates a Zn-specific structure with similar spacing as the dispersed feature in Ca-treated samples (SI Figure 8B). La L-III edge analysis showed a La feature with smaller spacing than those observed in Ca- and Zn-treated samples (SI Figure 8B). The presence of at least three different but stable states of pectin structure in Ca-, Zn-, and La-treated samples implies that pectin structure is modular and might be locally tuned by changes in ion abundance in the wall, resulting in nanoscale modification of cell wall organization.[9]

https://doi.org/10.1021/jacsau.3c00616
JACS Au 2024, 4, 177−188

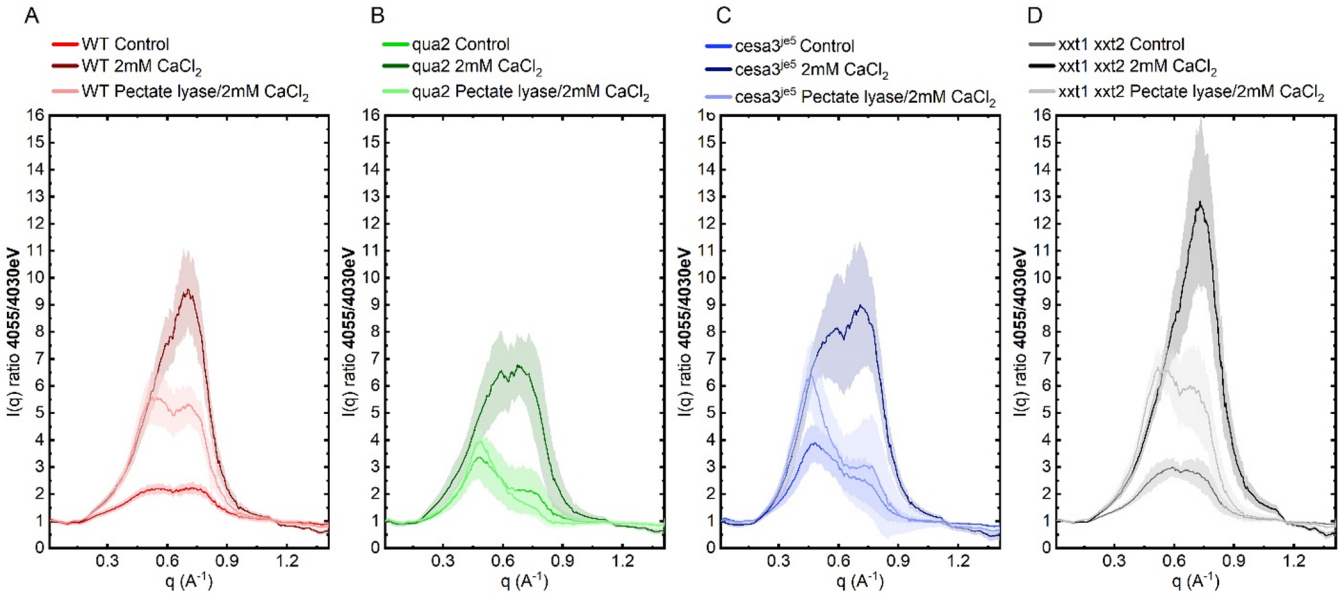

Figure 2. Ca-pectin structure is perturbed in wall component-deficient mutants. (A) $I(q)$ 4055/4030 eV ratios for WT (Ca and pectate lyase treated), (B) $I(q)$ 4055/4030 eV ratios for *qua2* pectin deficient mutant (Ca and pectate lyase treated), (C) $I(q)$ 4055/4030 eV ratios for *cesa3*^{je5} cellulose-deficient (Ca and pectate lyase treated), and (D) $I(q)$ 4055/4030 eV ratios for the *xxt1 xxt2* xyloglucan-deficient mutant (Ca and pectate lyase treated). Shaded color above and under curves shows standard deviation of $n > 9$ measurements from 3 independent samples made of >15 dry hypocotyls.

Together, these results suggest that there is a defined pectin structure that corresponds to spacing between polymer cross-linking sites, predominantly by Ca but also accessible to other cations. Moreover, alteration of this pectin structure by increasing or decreasing cross-linking appears to disorganize cellulose microfibrils (SI Figure 7A,B). Therefore, we next explored how pectin nanostructure is related to cellulose organization and asked whether changes in pectin nanostructure underpin the architectural and mechanical defects observed in cell wall-deficient mutants.[26−31]

Ca-HG Nanopatterning Supports the Structural Integrity of the Plant Cell Wall

To examine the biological significance of Ca-HG nanopatterning in the plant cell wall, we used TReXS to analyze *Arabidopsis* mutants deficient in pectin (*qua2*), cellulose (*cesa*^{je5}), and xyloglucan (*xxt1 xxt2*) and modulated pectin in those samples via addition of Ca or pectate lyase (plus its cofactor, Ca) to either saturate cross-linking or degrade pectin, respectively. For all genotypes, including a wild-type control, we observed a higher Ca-HG signal in Ca-treated samples and reduction of that signal after pectate lyase treatment (Figure 2). Moreover, in control conditions, the pectin- and cellulose-deficient mutants (*qua2* and *cesa*^{je5}, respectively) showed higher signal and reduced spacing in the range of the dispersed features (1.1−1.2 nm) and the Ca:polysaccharide signal (4075/4050 eV > 1) feature (1−6 nm) (SI Figures 9 and 10A−C). This implies that a deficiency in either pectin or cellulose disrupts Ca-HG nanopatterning *in muro*. It is possible that the increased signal arises from slightly thicker walls in those mutants because their elongation is restricted.[32] Reduction of the *d* spacing for the Ca feature in this case might also arise from reduced growth that prevents stretching of the cell wall and potentially the Ca-HG matrix. However, no changes in the condensed peak were observed between genotypes under control conditions or after Ca addition. This stability might simply arise from tighter packing of the Ca-HG structure, which could increase resistance to stretching. Alternatively, increased anisotropy along the longitudinal axis and potential association of this Ca-HG structure with cellulose might both increase resistance to deformation.

The spacing of the dispersed feature is larger in the *cesa3*^{je5} cellulose mutant than in WT, with or without addition of Ca (SI Figure 9B). Moreover, pectate lyase treatment led to a further increase in the spacing of the dispersed feature that approaches the spacing observed in pure Ca-pectin gel, suggesting a structural requirement for cellulose to establish the more tightly spaced, plant-specific Ca-HG structure (Figures 1F and 2C). The spacing of the condensed feature appears to be unaffected by Ca treatment in any of the genotypes (Figure 2). However, scattering intensity in the xyloglucan-deficient mutant was higher (without a change in spacing) after Ca treatment (Figure 2D), indicating an increased level of Ca-HG in this mutant[33] compared to WT and the other mutants. We also observed a decreased spacing in the condensed Ca-HG feature in the pectin-deficient *qua2* mutant upon pectate lyase treatment (Figure 2B), suggesting that sufficient pectin is critical to sustain normal Ca-HG nanopatterning in the cell wall. Accordingly, similar changes in all genotypes in untreated and pectate lyase-treated samples were observed for the Ca:polysaccharide signal (4075/4050 eV > 1) (SI Figure 10A−E). However, for the Ca treatment, the Ca:polysaccharide signal presented a new feature at ∼10 nm spacing that arose in WT, cellulose-deficient, and xyloglucan-deficient plants but not in pectin-deficient plants (SI Figure 10A−D,F). This feature was removed by pectate lyase treatment (SI Figure 10A−D,G). Together, the absence of a Ca treatment-dependent feature in the pectin mutant and its absence upon pectate lyase treatment suggest its Ca-HG origin. Interestingly, the pure Ca-pectin gel sample also had a peak in the 4075/4050 eV > 1 ratio at a scale of several nm (Figure 1G). This suggests that Ca treatment leads to *in muro* Ca-pectin gel cross-linking, and it seems that this gel becomes

https://doi.org/10.1021/jacsau.3c00616
JACS Au 2024, 4, 177−188

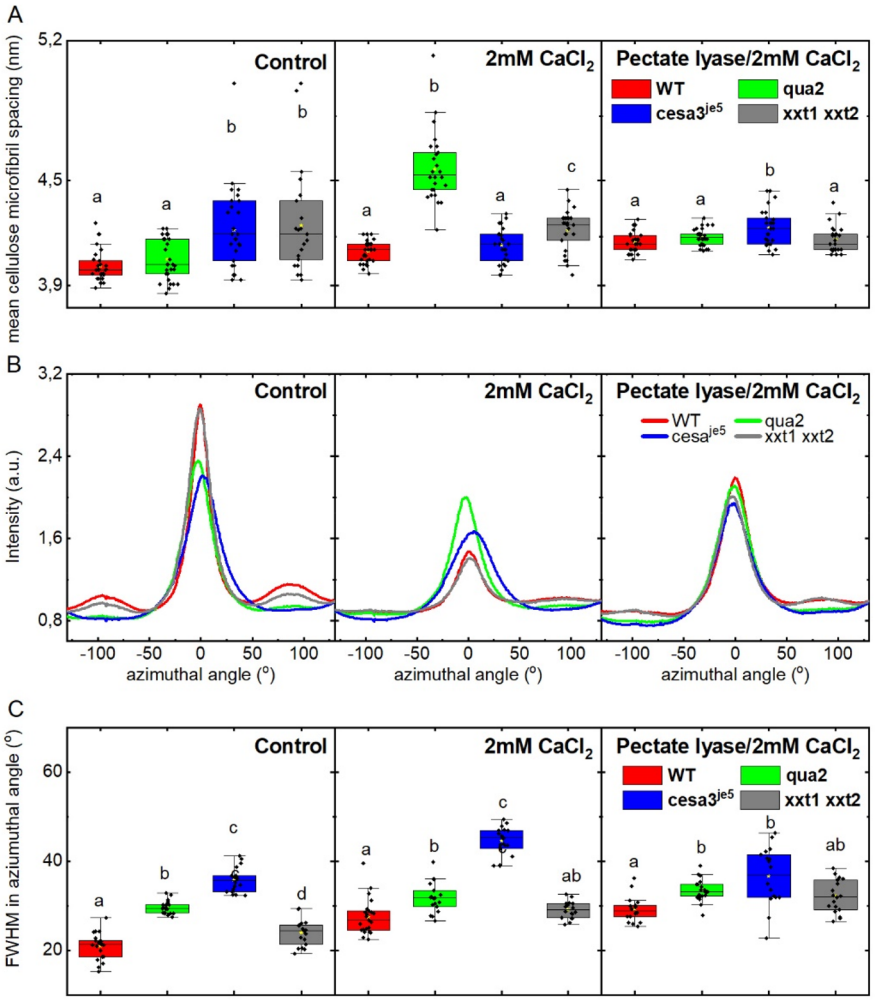

Figure 3. Modification of Ca-pectin in native walls affects cellulose microfibril spacing and arrangement. (A) Mean spacing between cellulose microfibrils in WT, *qua2*, *cesa3*^{je5}, and *xxt1 xxt2* plants under control, Ca, and pectate lyase treatment. (B) Integration along azimuthal angle of SAXS scattering images of WT, *qua2*, *cesa3*^{je5}, and *xxt1 xxt2* under control, Ca, and pectate lyase treatment. (C) Full width half-maximum (fwhm) of the main peak from SAXS scattering profiles obtained by integrating 2D data along the azimuthal angle for WT, *qua2*, *cesa3*^{je5}, and *xxt1 xxt2* under control, Ca, and pectate lyase treatment. Different letters (a, b, c) above boxes indicate statistically distinct groups, measured by one-way ANOVA with Tukey HSD, $p < 0.05$.

phase-separated from other wall components. This process of cellulose-pectin phase separation might help explain the emergence of the pectin-rich middle lamella during cell wall assembly and plant cell expansion.[34] Interestingly, extrusion of bacterial cellulose into highly Ca-cross-linked pectin led to pectin-cellulose phase separation.[35] Moreover, it seems that esterified, unbranched pectins do not mix well with highly branched, de-esterified pectins.[34] Finally, these results also suggest that pectin nanopatterning develops specifically during wall deposition and assembly and does not spontaneously arise from wall components being present together.

Cellulose Microfibril Spacing and Cellulose Bundle Organization Are Disrupted by Ca-HG Perturbation

Physical and functional cellulose-pectin interactions have been detected in previous studies.[31,36] We found that Driselase, chloroform, or genetically induced cellulose deficiency affects Ca-HG structure, possibly by disrupting interactions with cellulose (Figure 1, SI Figures 6 and 7). Therefore, we used TReXS to analyze cellulose spacing and alignment in wall-deficient mutants exposed to treatments that affect Ca-HG structure (Ca or pectate lyase treatment). Compared to wild-type controls, center-to-center spacing of cellulose microfibrils was larger in the cellulose-deficient *cesa3*^{je5} mutant with or without pectate lyase treatment, but not after Ca treatment (Figure 3A). This suggests that cellulose deficiency loosens wall architecture (Figure 3 and SI Figure 10) and that this architecture is Ca-HG-dependent. Additionally, Ca treatment caused increased cellulose spacing compared to untreated samples in wild-type and pectin-deficient seedlings (Figure 3A and SI Figure 11 insets in A, C, E, G). Adding Ca to samples might lead to increased cross-linking of demethylesterified sites in homogalacturonan chains. This could result in the disturbance of cellulose microfibril arrangement, with condensation of CMF structures where HG cross-linking occurs and increased spacing between other CMF that would spread apart. The characteristic peak of CMF at $q \sim 0.1-0.2$ Å^{-1} was broadened after Ca treatment (see SI Figure 11A,B and C,D, dark red compared to light red and dark green compared to light green, respectively). However, the broadening was not equal, showing an increased spacing range below 0.08 Å^{-1} in WT and 0.06 Å^{-1} in *qua2* compared to the region above 0.2 Å^{-1} in both WT and *qua2*. This might indicate that Ca binding

https://doi.org/10.1021/jacsau.3c00616
JACS Au 2024, 4, 177−188

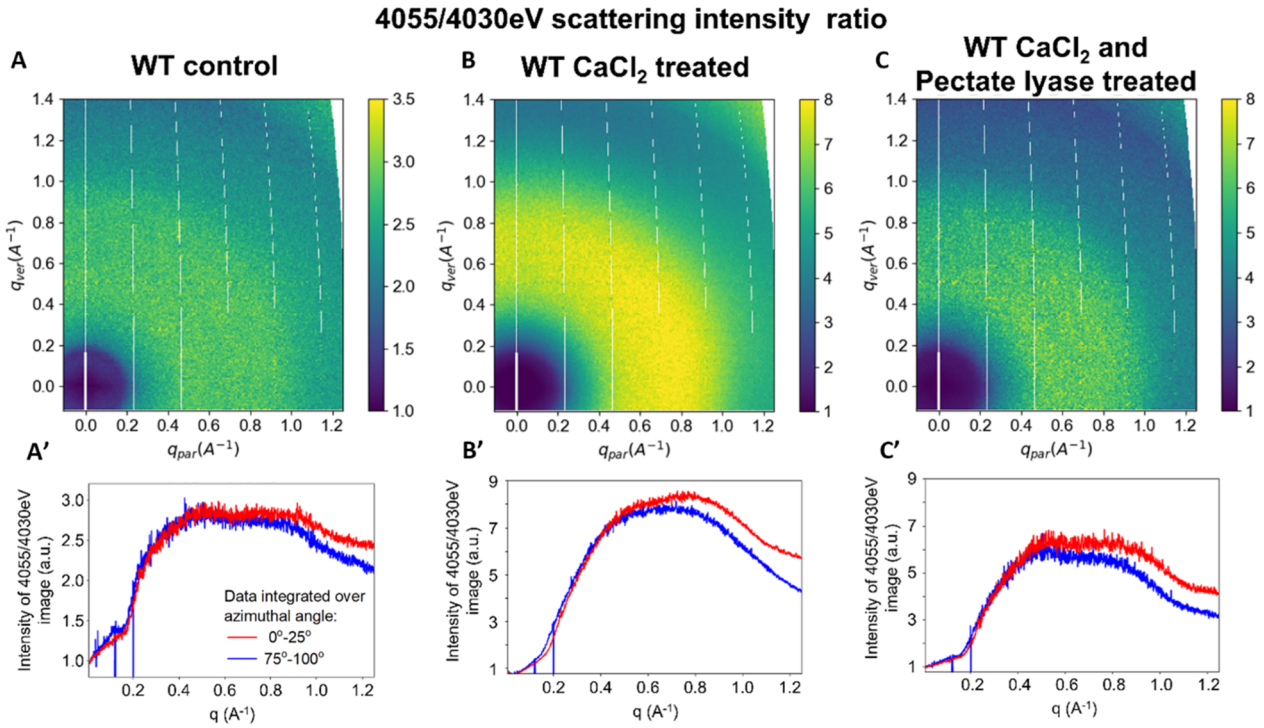

Figure 4. Ca-pectin structure with shorter spacing is anisotropic along the longitudinal axis of hypocotyls and microfibrils. (A−C) Scattering images of 4055/4030 eV ratio of WT control, Ca and pectate lyase treated samples, (A'−C') $I(q)$ 4055/4030 eV ratio profiles integrated at azimuthal angles of 0−25° (red) and 100−75° (blue); data correspond to scattering images A-C.

sites are not evenly distributed in the wall but rather clustered, causing a few CMF to become closer, which disturbs and loosens the arrangement of surrounding CMFs. The more pronounced effect in the *qua2* mutant is probably a result of its pectin deficiency. Pectate lyase treatment also led to significantly increased cellulose microfibril spacing in cellulose-deficient plants (SI Figure 11 inset in E), highlighting the essential function of Ca-HG in stabilizing the spacing interactions between cellulose microfibrils. The level of disturbance caused by deficiencies in cell wall components is also evident in differences in cellulose spacing peak size in pectin- and cellulose-deficient mutants (SI Figure 11).

X-ray scattering measurements performed with the detector positioned 5 m from the sample (Small Angle X-ray Scattering, SAXS) allow the detection of 12−600 nm structures and bulk estimation of cellulose bundle alignment in the wall.[3,16,22] SAXS azimuthal intensity profiles (I vs azimuthal angle, χ) from the same samples used for TReXS revealed cellulose alignment along the longitudinal growth axis of the hypocotyls (Figure 3B). We also used Full Width at Half-Maximum (fwhm) to further assess differences in cellulose bundle alignment (Figure 3C). The cellulose-deficient mutant had the most disrupted longitudinal bundle alignment and no visible peaks for transversely arranged bundles in all treatments (Figure 3B,C). In pectin-deficient plants, cellulose arrangement as measured by SAXS differed from the wild type under control, Ca or pectate lyase treatments. However, the effects of both treatments in the pectin-deficient mutant plants were similarly small, in contrast to the cellulose mutant, where Ca treatment increased the fwhm more than pectate lyase treatment (Figure 3C). This indicates that (i) pectins are critical for cellulose arrangement, and their reduction in *qua2* causes cellulose alignment to become less sensitive to Ca or pectate lyase treatments (Figure 3C); (ii) since Ca treatment alters cellulose alignment in all other genotypes, it appears that cellulose interacts with partially Ca-cross-linked pectin that can be further cross-linked by additional Ca. Pectin deficiency, similar to cellulose deficiency, led to reduced detection of transverse alignment under all treatments (Figure 3B). The lack of a signal for transverse microfibrils is surprising because both cellulose- and pectin-deficient plants show reduced growth, which given the transverse deposition of cellulose at the outer periclinal wall of the epidermis in unelongated cells,[6] would be expected to persist in these genotypes. However, the xyloglucan-deficient mutant had a prominent transverse peak and nearly (80%) wild-type growth (Figure 3B). These data suggest that cellulose-pectin interactions aid in the development of optimal cellulose bundling and multilamellate structures in the cell wall that are necessary for normal cell expansion.

In the xyloglucan-deficient mutant, we observed wider spacing between cellulose microfibrils than in wild-type in both control and Ca treatments but not after pectate lyase treatment (Figure 3A), suggesting that pectin might be responsible for changes in the control and Ca treatments.[37] Additionally, disruption of microfibril alignment in control conditions was "restored" to be similar to the wild type by affecting Ca-HG structure with Ca or pectate lyase treatment (Figure 3B and C). The *xxt1 xxt2* mutant has normal pectin content as estimated by GalA measurements,[38] but recent data suggest an increase in pectin content in this mutant;[37] in keeping with the latter result, our results show increased scattering signal from Ca-HG (Figure 2D) in *xxt1 xxt2* that seems to relate to disrupted cellulose spacing or bundle alignment, supporting the idea[38] that in the absence of xyloglucan, Ca-HG cross-linking might help support the structural integrity of the wall.

Together, the data presented above highlight direct interactions and structural interdependence between Ca-HG

https://doi.org/10.1021/jacsau.3c00616
JACS Au 2024, 4, 177−188

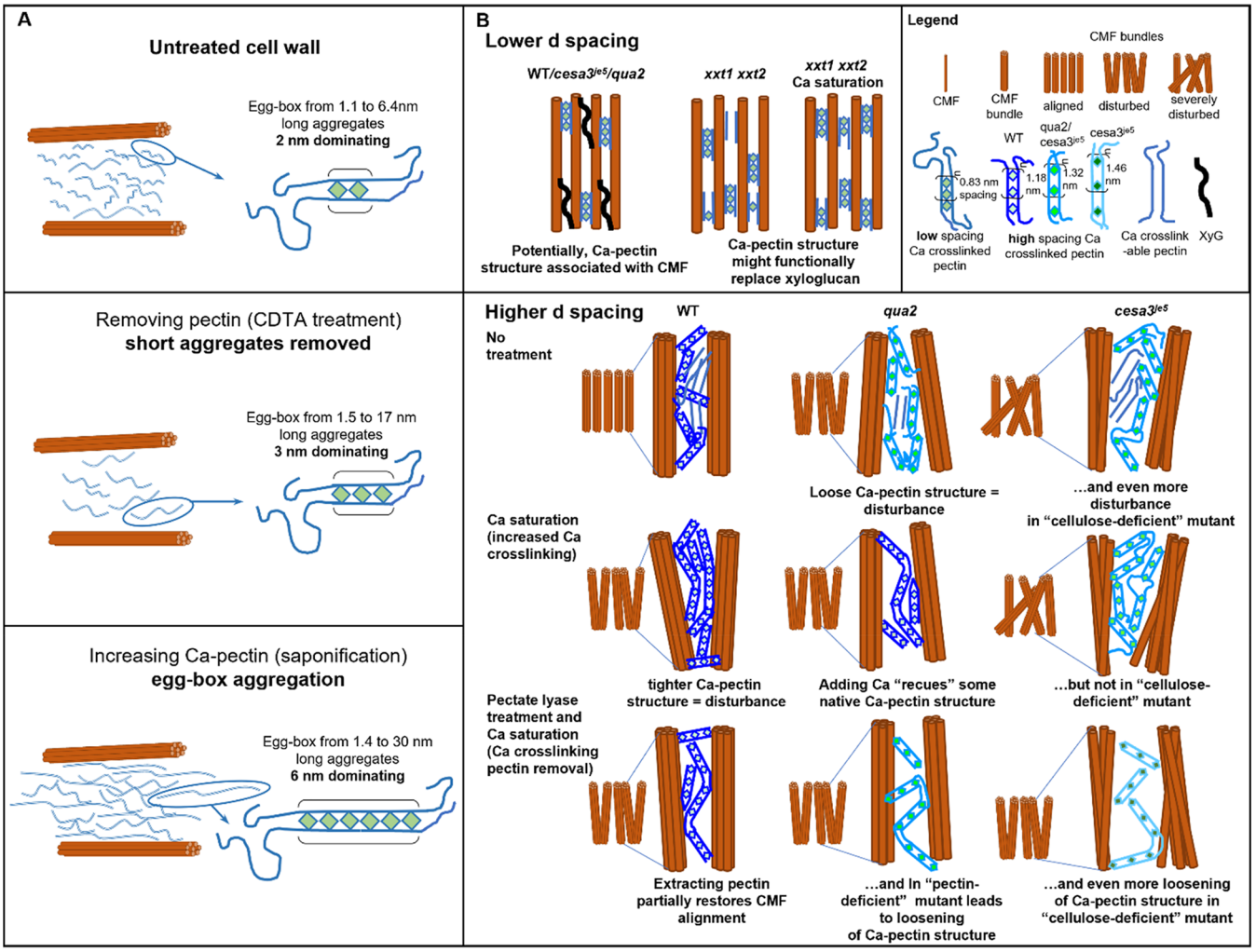

Figure 5. Graphical interpretation of results. Proposal of the Ca-pectin structure in WT hypocotyl primary cell wall after chemical treatments and its interaction with cellulose structure based on results of Ca-pectin structural changes, cellulose microfibril (CMF) spacing, and CMF bundle alignment in wall component-deficient mutants and following chemical/enzymatic treatments.

and cellulose microfibrils in native cell walls that are essential for their structural integrity.

Ca-HG Structures and Cellulose Microfibrils Have the Same Preferential Alignment

Finally, we found evidence of the mechanism underlying the ordering of Ca-HG structures in plant cell walls. We calculated ratios of on- and off-edge scattering images (4055 eV image/4030 eV image) to highlight potential anisotropy in Ca-HG structures. We detected increased scattering intensities for azimuthal angles along the longitudinal axes of hypocotyls (Figure 4A and A' red curve) for the condensed Ca-feature (above $q \sim 0.9$ 1 $Å^{-1}$ or 0.7 nm) in control conditions. Ca treatment led to similar but much stronger anisotropic enhancement of signal along the longitudinal axis of the hypocotyl, but at larger spacing $q \sim 0.68$ $Å^{-1}$ (0.92 nm) that corresponds to the disperse Ca-HG structure (Figure 4 and SI Figure 12). The anisotropic Ca-dependent structure and overall Ca signal were diminished by pectate lyase treatment, highlighting the necessity of pectin for the Ca-dependent structure (Figure 4). This suggests that the condensed features we detected might relate to Ca-HG structures in close proximity to other wall components (SI Figure 10) and that the structure that is relatively stable under treatments affecting Ca-HG (Figure 2, SI Figure 10) representing Ca-HG bound to cellulose microfibrils, possibly in contact with hemicelluloses. Furthermore, anisotropic alignment of the condensed Ca-HG feature corresponds to the dominant angle of cellulose alignment (SI Figure 2, Figure 3), indicating that cellulose microfibrils might provide a scaffold for this pectin structure, or vice versa. Because in the cellulose mutant there is no significant difference in intensity for signal integration along the longitudinal axis of the hypocotyl, and in the pectin mutant there is lower signal intensity in untreated hypocotyls and relatively higher signal after Ca treatment compared to other genotypes (SI Figure 12B–F), we suggest that although both components rely on each other, condensed pectin formation relies less on cellulose than dispersed pectin structure.

DISCUSSION

Here, we detected Ca order that is suggestive of flexible pectin nanopatterning in plant cell walls that can switch states depending on pectin content or cross-linking ion identity and found that this patterning is tightly interdependent with cellulose microfibril arrangement. In onion epidermal peels, Ca treatment leads to a dramatic increase in the elastic modulus of the pectin matrix and adding EDTA to chelate Ca and

https://doi.org/10.1021/jacsau.3c00616
JACS Au 2024, 4, 177–188

solubilize pectin results in a decreased modulus.[39,40] Enzymatic pectin demethylesterification results in wall softening,[40] indicating that Ca cross-linking is crucial for the ability of pectin to stiffen the wall. Our results indicate that increased Ca concentration leads to a specific cross-linking modality where nodes (Ca junctions in pectin polymers) move significantly closer to each other. This suggests that there is a fraction of uncross-linked, demethylesterified pectin that provides sites for potential cross-linking and might be tunable to influence wall stiffness (Figure 5). We found that applying different ions modifies pectin nanopatterning in ways that might affect wall mechanics and/or modify local wall properties during plant development. Indeed, Sariouglu et al.[41] showed that Zn-cross-linked pectin is more rigid than Ca-cross-linked pectin, which is a useful property for controlled drug delivery via tuning of pectin properties. Furthermore, Zn was less bioavailable and bound more strongly than Ca in citrus pectin.[42]

Ca-cross-linked pectin influences wall mechanical properties directly by stiffening the wall and also affects cellulose microfibril arrangement. Cellulose is the main load-bearing component of the cell wall,[43] but its arrangement is crucial in determining cell wall strength and the ability of a plant cell to expand anisotropically. Cellulose microfibril arrangement has been proposed to depend on the demethylesterification that allows for increased Ca binding.[4,44,45] For example, in puzzle piece-shaped epidermal pavement cells, lobe-neck morphogenesis is thought to be a consequence of asymmetric pectin demethylesterification that supports increased Ca binding and wall stiffening, in combination with changes in cellulose arrangement, on the wall segment where the neck is developing.[4] Additionally, in simplified analogs of cell walls assembled *in vitro* by growing cellulose (Iα)-producing bacteria (*Komagataeibacter xylinus*) in medium with or without calcium-cross-linked pectin, the calcium-cross-linked gel enhanced cellulose crystallinity and the compression resistance of the material. Interestingly, the mechanical properties of bacterial cellulose were unchanged when calcium-cross-linked pectin was introduced after the cellulose was synthesized,[46] implying that pectins influence the arrangement of cellulose during or shortly after its extrusion into the plant cell wall. The above evidence underlines the importance of Ca-cross-linked pectin in modulating cell wall properties. Our data further imply that normal pectin nanopatterning is crucial for proper cellulose organization. Digesting pectin with pectate lyase or increasing pectin cross-linking with Ca led to disruption of both the pectin and cellulose networks. The dispersed Ca-HG feature is impaired in *qua2* under control and pectate lyase treatments but is restored by Ca treatment, suggesting that Ca cross-linking is responsible for the self-organization of Ca-HG nanostructure. *qua2* mutants have significantly lower levels of both uronic acids and cellulose.[27] This might affect the way cellulose and pectin interact in these mutant walls, particularly in restricting Ca access for pectin cross-linking. In the *cesa3^{je5}* cellulose-deficient mutant, the dispersed feature is affected in the same way as in *qua2* but is not restored by Ca, suggesting more irreversible consequences of deficiencies in cellulose synthesis that nonetheless result in similar defects as those present in *qua2* pectin-deficient walls (Figure 5).

Finally, our results indicate that in xyloglucan-deficient *xxt1 xxt2* plants bulk cellulose and pectin organization remain largely unchanged. However, the signal indicating the relative level of Ca cross-linking is higher in the *xxt1 xxt2* mutant than in WT after Ca treatment (Figure 2), suggesting the presence of additional demethylesterified pectin. It has been suggested that in the *xxt1 xxt2* mutant, pectin interactions with cellulose increase and potentially structurally complement the loss of xyloglucan.[33,38] Our results allow us to more specifically hypothesize that the loss of xyloglucan is compensated for by an increase in pectin cross-linking nodes, which might take over some of the tethering function of xyloglucan (Figure 5). Pectins have been shown to function similarly in algae that lack extensive cellulose-xyloglucan networks,[47] and analogous functions might be achieved by cross-linkable arabinoxylans in grass cell walls, which can have low pectin abundance.[48]

The complexity of plant cell walls requires researchers to disentangle the properties and interactions of each component using a variety of methods, preferably in the context of intact walls. Here, we leveraged resonant X-ray scattering that allows for determination of the structural and chemical properties of wall components *in situ*. This allowed us to detect ordered Ca-containing structures that we associate with pectins that are assembled into Ca-HG nanostructures with specific spacing that are present only in intact cell walls. Damage to the pectin ultrastructure affects cellulose spacing and alignment, confirming the close functional relationships between these two wall components and suggesting that pectin structural failure might be a major factor in impairing the integrity and growth of wall-deficient plants. Moreover, we were able to point to Ca-HG assemblies as potential rescuing factors for wall integrity in xyloglucan-deficient plants. Among other uses, we see great potential in using TReXS to map the heterogeneity of pectin nanostructures and other chemically distinctive cell wall components, e.g., in lobes of pavement cells[9] or during tip growth,[5] to reveal the mechanisms underlying wall-directed cell morphogenesis in plants.

METHODS

Plant Material and Growth Conditions

We used *Arabidopsis thaliana* ecotype Colombia (Col), and three mutants deficient in cell wall components: cesa3^{je5} (mutation in *CELLULOSE SYNTHASE3*[30]), *qua2* (mutation in the *QUASIMODO2* pectin methyltransferase[27]) and *xxt1 xxt2* (mutation in *XYLOGLUCAN XYLOSYLTRANSFERASE1* and *2*[38]). Plants were surface sterilized using 30% (w/v) commercial bleach with 0.1% (w/v) SDS for 20 min, washed in sterile, deionized water at least four times, suspended in 0.15% agar solution, and stratified for 3 days at 4 °C in the dark. After stratification, seeds were sown on MS plates containing 2.2 g/L Murashige and Skoog salts (Caisson Laboratories), 0.6 g/L MES (Research Organics), 1% (w/v) sucrose, 0.8% (w/v) agar−agar (Research Organics), pH 5.6 and grown for 6 days in the dark (wrapped in aluminum foil) to generate elongated hypocotyls. Hypocotyls from at least four separate plates were pooled into single batches and stored at −80 °C until analysis.

Chemical Treatments

WT and mutant hypocotyls (independent batches) were treated with (i) 20 mM HEPES pH 7 incubated for 1 h (control), (ii) 2 mM $CaCl_2$ in 20 mM TRIS pH 9.5 for 16 h at 37 °C (Ca treatment), (iii) pectate lyase (Megazyme, 500 U/ml from *Cellvibrio japonicus*) in 20 mM TRIS pH 9.5 with 2 mM $CaCl_2$ (20 μL of enzyme/1 mL of buffer) and incubated for 16 h at 37 °C (Pectate Lyase treatment), (iv) Driselase in 20 mM sodium acetate buffer (pH 4.5) (100 μg powder/1 mL of buffer) incubated for 16 h in 37 °C (Driselase treatment), (v) chloroform was incubated for 72 h at room temperature (chloroform treatment), (vi) 50 mM cyclohexanediaminetetraacetic acid (CDTA) in 50 mM TRIS-base buffer, pH 7.2 incubated for 16 h at 37 °C (pectin extraction treatment − CDTA treatment), (vii) 2 M NaOH incubated for 16 h at 37 °C (saponification treatment − NaOH treatment), 2 mM $ZnSO_4$ or 2

https://doi.org/10.1021/jacsau.3c00616
JACS Au 2024, 4, 177−188

mM $LaCl_3$ in 20 mM TRIS, pH 9.5 for 16 h at 37 °C (Zn or Ln treatments). Buffers were chosen to allow for comparisons of TReXS data with earlier RSoXS studies[12] and for optimal pH buffering capacity. We confirmed that there is no significant difference in Ca feature presence and position between HEPES and TRIS buffer at the same pH of 7 and in comparison with acetate buffer at pH 4.5. Similarly, TRIS buffer at pH 7 or pH 9.5 did not significantly change the $I(q)$ profiles of $CaCl_2$ treated cell walls (SI Figure 13).

Gels and $CaCl_2$ Samples

Preparations of 1% low-methylesterified pectin (from citrus, Sigma-Aldrich) were made by mixing weighed amounts of pectin into heated (50−60 °C) milli-Q water and stirring them until dissolved. A final concentration of 2 mM $CaCl_2$ was added immediately before ∼10 mL of solution was poured onto Petri dishes with steel washers (5 mm inner diameter), which were left to dry at RT before being gently picked and placed on the TReXS sample holder. The 1% high-methylesterified (from apples, Sigma-Aldrich) pectin gel (HM gel) was made by mixing pectin into 55% w/v sucrose in water at pH 3.5, stirring until mixed (with gentle heating), poured on Petri dishes (to make a 1.5−2 mm layer) and left to dry. Small strips of gel were placed on a sample holder. The $CaCl_2$ sample was prepared by drop-casting a $CaCl_2$ solution onto silicon nitride widows (50 nm thick, Norcada) and air drying.

NEXAFS and TReXS Measurements

Scattering measurements and analyses were performed at Brookhaven National Laboratory, National Synchrotron Light Source II, at beamline 12-ID SMI. We used two detectors in order to cover a wide q-range: (i) a WAXS Pilatus 300 KW detector positioned at 0.2739 m from the sample, where the q-range was obtained by rotating the detector around the sample at a fixed arc, and (ii) a SAXS Pilatus 1 M detector positioned at 5 m from the sample. Fluorescence NEXAFS spectra were recorded using the Pilatus 300 KW detector positioned at an angle of 55° by scanning the energy from 4030 to 4150 eV with 1 eV resolution using 1 s exposures. The WAXS and SAXS measurements were performed at 4030, 4040, 4050, 4055, and 4075 eV. The fwhm of the beam was 50 × 200 μm (HxV) with the vertical diameter aligned with the hypocotyl elongation axis. Samples were placed and fixed with vacuum epoxy (Torr Seal) onto a 3 mm diameter aluminum sample holder arm. Samples were air-dried on the sample holder to facilitate TReXS measurements that are performed under vacuum. Each sample was made from batches of ∼20 aligned hypocotyls. The lower middle (1−2 mm from roots) regions of the hypocotyls were used as measurement targets. A systematic offset of ∼3 eV between the energy values from the beamline and the expected calibrated values was observed. Since the NEXAFS and TReXS data were obtained with the same energy offset, this offset does not affect the interpretation of the results.

Data Analysis

Raw detector images were converted in the reciprocal space using the SMI analysis package in Jupyter notebook (https://jupyter.org) and xi-cam software.[49] WAXS data were radially integrated along azimuthal angles from −90° to 10°. SAXS data were azimuthally integrated (−135° to 135°) to highlight alignment in the longitudinal orientation (0°). Analysis of the signal along the longitudinal (0°) and transverse (90°) direction to the hypocotyl axis was performed by azimuthal integration from (i) 0−25° and 75−100° for the division of the scattering images and (i) 5−25° and 60−90° for $I(q)$ profiles. After integration, the fluorescent background was extracted by subtracting the 95% value of the lowest $I(q)$ intensity from the q 0.9−0.6 ($Å^{-1}$) region. Integrated and background subtracted data were analyzed with OriginPro 2019−2021 (OriginLab) using peak and baseline analyzer to find the cutoff baseline and particular peaks.

d-spacing (d) was calculated from the scattering vector, q, using a Bragg's law-derived dependency: $d = 2\pi/q$.

The $I(q)$ data division (4055 eV/4030 eV) was made using python standard packages (numpy, fabio, os, scipy, etc.), divided signal smoothing was made using Savitzky-Golay filter with second polynomial order and window length of 55 (savgol_filter, scipy), and calculations were made in Jupyter notebook (https://jupyter.org) and Excel (Microsoft).

All data for each treatment condition were analyzed using the same settings (batch analysis) and supervised for artifacts. Common artifacts included hypocotyl breaking/misalignment or foreign material (dust, metal peaks from the holder, etc.). If artifacts were present, measurements were removed from analysis. For each treatment/experiment, at least nine samples from at least three biological replicates (three separate beamtimes) were used. Gels and $CaCl_2$ samples were prepared in triplicate (one beamtime).

Means and statistical analyses were computed with the Xrealstats (www.real-statistics.com) add-in in Excel (Microsoft); significance was assessed using one-way ANOVA ($p < 0.05$, Bonferroni correction), with Tukey HSD and pairwise t test as follow-up.

Theoretical Prediction of Scattering Contrast Profiles and Total Scattering Intensity (TSI)

Theoretical prediction of scattering contrast and TSI rationale are described in Ye et al.[12] Briefly, scattering contrast was calculated based on a previously derived formula:[19,20]

$$\text{scattering contrast} = \frac{(\Delta\delta^2 + \Delta\beta^2)}{\lambda^4}$$

where λ is the beam wavelength, δ is the dispersive component, and β is the absorptive component of the refractive index of individual components in a sample/material.

Calculation of refractive indices δ from β of each material in the 4030−4150 eV X-ray region of the spectrum from measured NEXAFS absorption data[12] or predicted from the chemical composition[21] via the Kramers−Kronig transform was done using kkcalc 0.8.1.

The predicted composite component was calculated by summing fractions (totaling to 100%) of each material's predicted scattering contrast for the specific energy used. We calculated the contrast between the following fractions: Pectin without Ca cross-linking vs calcium as $CaCl_2$ (Pectin − $CaCl_2$); Pectin without Ca cross-linking vs pectin cross-linked with $CaCl_2$ (Pectin − Ca-pectin); Cellulose vs pectin cross-linked with $CaCl_2$ (Cellulose − Ca-pectin); Pectin cross-linked with $CaCl_2$ vs vacuum (Ca-pectin−vacuum); Cellulose vs hemicellulose (Cellulose−hemicellulose); Cellulose vs pectin without Ca cross-linking (Cellulose−pectin); Hemicellulose vs pectin without Ca cross-linking (Hemicellulose−pectin); Pectin without Ca cross-linking vs vacuum (Pectin−vacuum); Cellulose vs hemicellulose (Cellulose−hemicellulose).

TSI was calculated from TReXS acquired data (q-range 0.01−1.41 A^{-1}) for WT hypocotyls and pectin gel cross-linked by calcium. We normalized scattering data by the direct beam flux, exposure time, and sample transmittance and then calculated TSI as $\int I(q)q^2dq$.

■ ASSOCIATED CONTENT

Supporting Information

The Supporting Information is available free of charge at https://pubs.acs.org/doi/10.1021/jacsau.3c00616.

NEXAFS profiles of untreated (control) and 2 mM $CaCl_2$ treated WT hypocotyls; WAXS images at 4055 and 4030 eV and SAXS images at 4055 eV; scattering intensity profile at 4055 eV for untreated WT hypocotyls integrated at different azimuthal angles; hard X-ray scattering data for WT and mutant hypocotyls; theoretical scattering contrast and data for total scattering intensities at different q-ranges for Ca-pectin, *Arabidopsis* hypocotyls and $CaCl_2$; $I(q)$ 4055/4030 eV and 4075/4050 eV ratio for WT control, WT hypocotyls incubated in NaOH (saponification), chloroform (72 h, nonpolar solvent), Driselase (cell wall digesting enzymes), highly methylesterified pectin and $CaCl_2$; TReXS $I(q)$ profiles for WT hypocotyls untreated and treated with chloroform and Driselase, CDTA, NaOH

https://doi.org/10.1021/jacsau.3c00616
JACS Au 2024, 4, 177−188

and for low methylesterified (LM) gels with different levels of Ca and high methylesterified pectin gel; $I(q)$ 4055/4030 eV ratio for Zn and La treated samples, $I(q)$ 9670/9640 eV (Zn K-edge) of Zn treated sample, $I(q)$ 4055/4030 eV ratio for Ca treated sample and $I(q)$ 5495/5460 eV ratio for La treated sample; quantification of Figure 2 data; $I(q)$ 4075/4050 eV ratios for Ca and pectate lyase treated: WT, *cesa3je5*, *qua2*, and *xxt1 xxt2*; TReXS $I(q)$ raw and offset profiles of untreated, Ca treated, and pectate lyase treated WT, *qua2*, *cesa3je5*, and *xxt1 xxt2*; $I(q)$ 4055/4030 eV ratios of untreated and Ca treated WT, *qua2*, *cesa3je5*, and *xxt1 xxt2* at different azimuthal angles; $I(q)$ 4055/4030 eV ratios for WT untreated and treated hypocotyls using buffers HEPES (pH7), TRIS (pH7 and 9) acetic buffer (4,5) and WT Driselase treated in acetate buffer (pH 4.5) (PDF)

AUTHOR INFORMATION

Corresponding Authors

Oskar Siemianowski − *Department of Biology, The Pennsylvania State University, University Park, Pennsylvania 16802, United States; Faculty of Biology, Institute of Experimental Plant Biology and Biotechnology, University of Warsaw, 02-096 Warszawa, Poland*; Email: o.siemianowski@uw.edu.pl

Charles T. Anderson − *Department of Biology, The Pennsylvania State University, University Park, Pennsylvania 16802, United States*; orcid.org/0000-0001-7481-3571; Email: cta3@psu.edu

Authors

Sintu Rongpipi − *Department of Chemical Engineering, The Pennsylvania State University, University Park, Pennsylvania 16802, United States*; orcid.org/0000-0002-5979-4533

Joshua T. Del Mundo − *Department of Chemical Engineering, The Pennsylvania State University, University Park, Pennsylvania 16802, United States*

Guillaume Freychet − *National Synchrotron Light Source II, Brookhaven National Laboratory, Upton, New York 11973, United States*

Mikhail Zhernenkov − *National Synchrotron Light Source II, Brookhaven National Laboratory, Upton, New York 11973, United States*; orcid.org/0000-0003-3604-0672

Enrique D. Gomez − *Department of Chemical Engineering and Department of Materials Science and Engineering and Materials Research Institute, The Pennsylvania State University, University Park, Pennsylvania 16802, United States*; orcid.org/0000-0001-8942-4480

Esther W. Gomez − *Department of Chemical Engineering and Department of Biomedical Engineering, The Pennsylvania State University, University Park, Pennsylvania 16802, United States*; orcid.org/0000-0003-2082-013X

Complete contact information is available at: https://pubs.acs.org/10.1021/jacsau.3c00616

Notes

The authors declare no competing financial interest.

ACKNOWLEDGMENTS

This work was supported as part of The Center for Lignocellulose Structure and Formation, an Energy Frontier Research Center funded by the U.S. Department of Energy, Office of Science, Basic Energy Sciences under Award # DE-SC0001090. This research used the Soft Matter Interfaces Beamline (SMI, Beamline 12-ID) of the National Synchrotron Light Source II, a U.S. Department of Energy (DOE) Office of Science User Facility operated for the DOE Office of Science by Brookhaven National Laboratory under Contract No. DE-SC0012704.

REFERENCES

(1) Wang, Y.; Jiao, Y. Cellulose Microfibril-Mediated Directional Plant Cell Expansion: Gas and Brake. *Mol. Plant* **2020**, *13* (12), 1670−1672.

(2) Balat, M.; Ayar, G. Biomass energy in the world, use of biomass and potential trends. *Energy sources* **2005**, *27* (10), 931−940.

(3) Rongpipi, S.; Ye, D.; Gomez, E. D.; Gomez, E. W. Progress and Opportunities in the Characterization of Cellulose - An Important Regulator of Cell Wall Growth and Mechanics. *Front Plant Sci.* **2019**, *9*, 1894.

(4) Altartouri, B.; Bidhendi, A. J.; Tani, T.; Suzuki, J.; Conrad, C.; Chebli, Y.; Liu, N.; Karunakaran, C.; Scarcelli, G.; Geitmann, A. Pectin chemistry and cellulose crystallinity govern pavement cell morphogenesis in a multi-step mechanism. *Plant Physiol.* **2019**, *181* (1), 127−141.

(5) Dehors, J.; Mareck, A.; Kiefer-Meyer, M. C.; Menu-Bouaouiche, L.; Lehner, A.; Mollet, J. C. Evolution of Cell Wall Polymers in Tip-Growing Land Plant Gametophytes: Composition, Distribution, Functional Aspects and Their Remodeling. *Front Plant Sci.* **2019**, *10*, 441.

(6) Crowell, E. F.; Timpano, H.; Desprez, T.; Franssen-Verheijen, T.; Emons, A. M.; Hofte, H.; Vernhettes, S. Differential regulation of cellulose orientation at the inner and outer face of epidermal cells in the Arabidopsis hypocotyl. *Plant Cell* **2011**, *23* (7), 2592−605.

(7) Leppard, G. G.; Colvin, J. R. Electron-opaque fibrils and granules in and between the cell walls of higher plants. *J. Cell Biol.* **1972**, *53* (3), 695−703.

(8) Walkinshaw, M. D.; Arnott, S. Conformations and interactions of pectins. II. Models for junction zones in pectinic acid and calcium pectate gels. *J. Mol. Biol.* **1981**, *153* (4), 1075−85.

(9) Haas, K. T.; Wightman, R.; Meyerowitz, E. M.; Peaucelle, A. Pectin homogalacturonan nanofilament expansion drives morphogenesis in plant epidermal cells. *Science* **2020**, *367* (6481), 1003−1007.

(10) Cosgrove, D. J.; Anderson, C. T. Plant Cell Growth: Do Pectins Drive Lobe Formation in Arabidopsis Pavement Cells? *Curr. Biol.* **2020**, *30* (11), R660−R662.

(11) Rongpipi, S.; Del Mundo, J. T.; Gomez, E. D.; Gomez, E. W. Extracting structural insights from soft X-ray scattering of biological assemblies. In *Methods in Enzymology*; Elsevier: 2023; Vol. *678*, pp 121−144.

(12) Ye, D.; Kiemle, S. N.; Rongpipi, S.; Wang, X.; Wang, C.; Cosgrove, D. J.; Gomez, E. W.; Gomez, E. D. Resonant soft X-ray scattering reveals cellulose microfibril spacing in plant primary cell walls. *Sci. Rep* **2018**, *8* (1), 12449.

(13) Rongpipi, S.; Barnes, W. J.; Siemianowski, O.; Del Mundo, J. T.; Wang, C.; Freychet, G.; Zhernenkov, M.; Anderson, C. T.; Gomez, E. W.; Gomez, E. D. Measuring calcium content in plants using NEXAFS spectroscopy. *Frontiers in Plant Science* **2023**, *14*, 1212126.

(14) Kennedy, C. J.; Cameron, G. J.; Šturcová, A.; Apperley, D. C.; Altaner, C.; Wess, T. J.; Jarvis, M. C. Microfibril diameter in celery collenchyma cellulose: X-ray scattering and NMR evidence. *Cellulose* **2007**, *14* (3), 235−246.

(15) Fernandes, A. N.; Thomas, L. H.; Altaner, C. M.; Callow, P.; Forsyth, V. T.; Apperley, D. C.; Kennedy, C. J.; Jarvis, M. C. Nanostructure of cellulose microfibrils in spruce wood. *Proc. Natl. Acad. Sci. U. S. A.* **2011**, *108* (47), E1195−203.

(16) Saxe, F.; Eder, M.; Benecke, G.; Aichmayer, B.; Fratzl, P.; Burgert, I.; Rüggeberg, M. Measuring the distribution of cellulose microfibril angles in primary cell walls by small angle X-ray scattering. *Plant Methods* **2014**, *10* (1), 25.
(17) Sponsler, O.; Dore, W. In *The structure of ramie cellulose as derived from X-ray data*; Fourth Colloid Symposium Monograph, 1926; pp 174−202.
(18) Meyer, K. H.; Mark, H. Über den Bau des krystallisierten Anteils der Cellulose. *Berichte der deutschen chemischen Gesellschaft (A and B Series)* **1928**, *61* (4), 593−614.
(19) Henke, B. L.; Gullikson, E. M.; Davis, J. C. X-ray interactions: photoabsorption, scattering, transmission, and reflection at E= 50−30,000 eV, Z= 1−92. *Atomic data and nuclear data tables* **1993**, *54* (2), 181−342.
(20) de L. Kronig, R. On the theory of dispersion of X-rays. *Josa* **1926**, *12* (6), 547−557.
(21) Watts, B. Calculation of the Kramers-Kronig transform of X-ray spectra by a piecewise Laurent polynomial method. *Opt. Express* **2014**, *22* (19), 23628−23639.
(22) Penttila, P. A.; Altgen, M.; Awais, M.; Osterberg, M.; Rautkari, L.; Schweins, R. Bundling of cellulose microfibrils in native and polyethylene glycol-containing wood cell walls revealed by small-angle neutron scattering. *Sci. Rep* **2020**, *10* (1), 20844.
(23) Temple, H.; Phyo, P.; Yang, W.; Lyczakowski, J. J.; Echevarria-Poza, A.; Yakunin, I.; Parra-Rojas, J. P.; Terrett, O. M.; Saez-Aguayo, S.; Dupree, R.; Orellana, A.; Hong, M.; Dupree, P. Golgi-localized putative S-adenosyl methionine transporters required for plant cell wall polysaccharide methylation. *Nat. Plants* **2022**, *8* (6), 656−669.
(24) Ha, M.-A.; Evans, B.; Apperley, D.; Jarvis, M. Rigid and flexible pectic polymers in onion cell walls. In *Progress in Biotechnology*; Elsevier: 1996; Vol. *14*, pp 561−568.
(25) Culp, T. E.; Ye, D.; Paul, M.; Roy, A.; Behr, M. J.; Jons, S.; Rosenberg, S.; Wang, C.; Gomez, E. W.; Kumar, M.; Gomez, E. D. Probing the Internal Microstructure of Polyamide Thin-Film Composite Membranes Using Resonant Soft X-ray Scattering. *ACS Macro Lett.* **2018**, *7* (8), 927−932.
(26) Perez Garcia, M.; Zhang, Y.; Hayes, J.; Salazar, A.; Zabotina, O. A.; Hong, M. Structure and interactions of plant cell-wall polysaccharides by two- and three-dimensional magic-angle-spinning solid-state NMR. *Biochemistry* **2011**, *50* (6), 989−1000.
(27) Du, J.; Kirui, A.; Huang, S.; Wang, L.; Barnes, W. J.; Kiemle, S.; Zheng, Y.; Rui, Y.; Ruan, M.; Qi, S.; Kim, S. H.; Wang, T.; Cosgrove, D. J.; Anderson, C. T.; Xiao, C. Mutations in the Pectin Methyltransferase QUASIMODO2 Influence Cellulose Biosynthesis and Wall Integrity in Arabidopsis thaliana. *Plant Cell* **2020**, *32*, 3576.
(28) Xiao, C.; Zhang, T.; Zheng, Y.; Cosgrove, D. J.; Anderson, C. T. Xyloglucan Deficiency Disrupts Microtubule Stability and Cellulose Biosynthesis in Arabidopsis, Altering Cell Growth and Morphogenesis. *Plant Physiol.* **2016**, *170* (1), 234−49.
(29) Park, Y. B.; Cosgrove, D. J. Changes in Cell Wall Biomechanical Properties in the Xyloglucan-Deficient xxt1/xxt2Mutant of Arabidopsis. *Plant Physiol.* **2012**, *158* (1), 465−75.
(30) Desprez, T.; Juraniec, M.; Crowell, E. F.; Jouy, H.; Pochylova, Z.; Parcy, F.; Hofte, H.; Gonneau, M.; Vernhettes, S. Organization of cellulose synthase complexes involved in primary cell wall synthesis in Arabidopsis thaliana. *Proc. Natl. Acad. Sci. U. S. A.* **2007**, *104* (39), 15572−7.
(31) Kirui, A.; Du, J.; Zhao, W.; Barnes, W.; Kang, X.; Anderson, C. T.; Xiao, C.; Wang, T. A pectin methyltransferase modulates polysaccharide dynamics and interactions in Arabidopsis primary cell walls: Evidence from solid-state NMR. *Carbohydr. Polym.* **2021**, *270*, No. 118370.
(32) Derbyshire, P.; Findlay, K.; McCann, M. C.; Roberts, K. Cell elongation in Arabidopsis hypocotyls involves dynamic changes in cell wall thickness. *J. Exp Bot* **2007**, *58* (8), 2079−89.
(33) Sowinski, E. E.; Westman, B. M.; Redmond, C. R.; Kong, Y.; Olek, A. T.; Olek, J.; McCann, M. C.; Carpita, N. C. Lack of xyloglucan in the cell walls of the Arabidopsis xxt1/xxt2 mutant results in specific increases in homogalacturonan and glucomannan. *Plant Journal* **2022**, *110*, 212.
(34) MacDougall, A. J.; Rigby, N. M.; Ring, S. G. Phase separation of plant cell wall polysaccharides and its implications for cell wall assembly. *Plant Physiol.* **1997**, *114* (1), 353−362.
(35) Chanliaud, E.; Gidley, M. J. In vitro synthesis and properties of pectin/Acetobacter xylinus cellulose composites. *Plant J.* **1999**, *20* (1), 25−35.
(36) Du, J.; Kirui, A.; Huang, S.; Wang, L.; Barnes, W. J.; Kiemle, S. N.; Zheng, Y.; Rui, Y.; Ruan, M.; Qi, S.; Kim, S. H.; Wang, T.; Cosgrove, D. J.; Anderson, C. T.; Xiao, C. Mutations in the Pectin Methyltransferase QUASIMODO2 Influence Cellulose Biosynthesis and Wall Integrity in Arabidopsis. *Plant Cell* **2020**, *32* (11), 3576−3597.
(37) Sowinski, E. E.; Westman, B. M.; Redmond, C. R.; Kong, Y.; Olek, A. T.; Olek, J.; McCann, M. C.; Carpita, N. C. Lack of xyloglucan in the cell walls of the Arabidopsis xxt1/xxt2 mutant results in specific increases in homogalacturonan and glucomannan. *Plant J.* **2022**, *110* (1), 212−227.
(38) Cavalier, D. M.; Lerouxel, O.; Neumetzler, L.; Yamauchi, K.; Reinecke, A.; Freshour, G.; Zabotina, O. A.; Hahn, M. G.; Burgert, I.; Pauly, M.; Raikhel, N. V.; Keegstra, K. Disrupting two Arabidopsis thaliana xylosyltransferase genes results in plants deficient in xyloglucan, a major primary cell wall component. *Plant Cell* **2008**, *20* (6), 1519−37.
(39) Xi, X.; Kim, S. H.; Tittmann, B. Atomic force microscopy based nanoindentation study of onion abaxial epidermis walls in aqueous environment. *J. Appl. Phys.* **2015**, *117* (2), No. 024703.
(40) Wang, X.; Wilson, L.; Cosgrove, D. J. Pectin methylesterase selectively softens the onion epidermal wall yet reduces acid-induced creep. *J. Exp Bot* **2020**, *71* (9), 2629−2640.
(41) Sarioglu, E.; Arabacioglu Kocaaga, B.; Turan, D.; Batirel, S.; Guner, F. S. Theophylline-loaded pectin-based hydrogels. II. Effect of concentration of initial pectin solution, crosslinker type and cation concentration of external solution on drug release profile. *J. Appl. Polym. Sci.* **2019**, *136* (43), 48155.
(42) Celus, M.; Kyomugasho, C.; Salvia-Trujillo, L.; Van Audenhove, J.; Van Loey, A. M.; Grauwet, T.; Hendrickx, M. E. Interactions between citrus pectin and Zn2+ or Ca2+ and associated in vitro Zn2+ bioaccessibility as affected by degree of methylesterification and blockiness. *Food Hydrocolloids* **2018**, *79*, 319−330.
(43) Zhang, Y.; Yu, J.; Wang, X.; Durachko, D. M.; Zhang, S.; Cosgrove, D. J. Molecular insights into the complex mechanics of plant epidermal cell walls. *Science* **2021**, *372* (6543), 706−711.
(44) Peaucelle, A.; Wightman, R.; Höfte, H. The Control of Growth Symmetry Breaking in the *Arabidopsis* Hypocotyl. *Curr. Biol.* **2015**, *25* (13), 1746−1752.
(45) Bou Daher, F.; Chen, Y.; Bozorg, B.; Clough, J.; Jönsson, H.; Braybrook, S. A. Anisotropic growth is achieved through the additive mechanical effect of material anisotropy and elastic asymmetry. *Elife* **2018**, *7*, No. e38161.
(46) Lopez-Sanchez, P.; Martinez-Sanz, M.; Bonilla, M. R.; Wang, D.; Gilbert, E. P.; Stokes, J. R.; Gidley, M. J. Cellulose-pectin composite hydrogels: Intermolecular interactions and material properties depend on order of assembly. *Carbohydr. Polym.* **2017**, *162*, 71−81.
(47) Boyer, J. S. Enzyme-Less Growth in *Chara* and Terrestrial Plants. *Front Plant Sci.* **2016**, *7*, 866.
(48) Vogel, J. Unique aspects of the grass cell wall. *Curr. Opin. Plant Biol.* **2008**, *11* (3), 301−7.
(49) Pandolfi, R. J.; Allan, D. B.; Arenholz, E.; Barroso-Luque, L.; Campbell, S. I.; Caswell, T. A.; Blair, A.; De Carlo, F.; Fackler, S.; Fournier, A. P.; et al. Xi-cam: a versatile interface for data visualization and analysis. *Journal of Synchrotron Radiation* **2018**, *25* (4), 1261−1270.

https://doi.org/10.1021/jacsau.3c00616
JACS Au 2024, 4, 177−188